LOW-ENERGY SPUTTERING STUDIES

By

DANIEL McKEOWN, AMADO CABEZAS

AND EDWARD T. MACKENZIE

14 July 1961

Annual Report

15 July 1960 to 14 July 1961

Principal Investigator, D. McKeown

Contract Nonr - 3157 (00), Task NR012-403

Department of the Navy

Office of Naval Research

Washington 25, D. C.

GD

GENERAL DYNAMICS

ASTRONAUTICS

DISCLAIMER

This report was prepared as an account of work sponsored by an agency of the United States Government. Neither the United States Government nor any agency thereof, nor any of their employees, makes any warranty, express or implied, or assumes any legal liability or responsibility for the accuracy, completeness, or usefulness of any information, apparatus, product, or process disclosed, or represents that its use would not infringe privately owned rights. Reference herein to any specific commercial product, process, or service by trade name, trademark, manufacturer, or otherwise does not necessarily constitute or imply its endorsement, recommendation, or favoring by the United States Government or any agency thereof. The views and opinions of authors expressed herein do not necessarily state or reflect those of the United States Government or any agency thereof.

DISCLAIMER

Portions of this document may be illegible in electronic image products. Images are produced from the best available original document.

TABLE OF CONTENTS

	Page
TABLE OF CONTENTS	i
LIST OF ILLUSTRATIONS	ii
ABSTRACT	1
INTRODUCTION	1
EXPERIMENTAL METHOD	2
EXPERIMENTAL RESULTS	20
COMPARISON WITH OTHER RELATED EXPERIMENTS	26
DISCUSSION OF SPUTTERING THEORIES	29
ANALYSIS OF RESULTS	30
ACKNOWLEDGEMENTS	38
BIBLIOGRAPHY	39

LIST OF ILLUSTRATIONS

		Page
Figure 1.	Ion beam generator	4
2.	Beam current as a function of target voltage.	5
3.	Energy spread of the beam	6
4.	Experimental apparatus	8
5.	Beam generator	9
6.	Target chamber	10
7.	10-Mc crystal resonator	12
8.	Evaporator unit for plating quartz. . . . crystals	13
9.	Crystal equivalent electrical circuit . .	17
10.	Equivalent circuit admittance plot . . .	18
11.	10-Mc crystal oscillator	19
12.	20-Mc crystal frequency change as a function of beam energy	22
13.	Sputtering rates of gold in noble gases between 0 and 100 ev	23
14.	Sputtering rates of gold in noble gases between 100 and 1000 ev	24
15.	Sputtering rates of aluminum in noble gases between 100 and 1000 ev.	25
16.	Comparison of sputtering yields with other measurements	27
17.	Secondary electron and sputtering yields for molybdenum in neon	28

Page

Figure 18. Schematic yield curve for various bombarding beam energies 32

19. Plot of the energy transfer coefficient η, $\frac{4mM}{(m+M)^2}$, for gold and aluminum 34

20. Sputtering yield of gold as a function of the atomic weight of the bombarding gas 35

21. Sputtering yield of aluminum as a function of the atomic weight of the bombarding gas 36

LOW-ENERGY SPUTTERING STUDIES

Daniel McKeown
Amado Cabezas
Edward T. MacKenzie

ABSTRACT

A study has been made on the sputtering of gold and aluminum in beams of noble gases at normal incidence between 0 and 1000 ev. Gold was bombarded by He^+, Ne^+, Ar^+, and Xe^+, and aluminum by Ne^+, Ar^+, and Kr^+. Sputtering was measured by the crystal oscillator method. Using 20-Mc crystals in the oscillator, it was possible to detect the average sputtering of 0.01 angstrom from a surface. Secondary electron emission from the target was suppressed, and sputtering yields, μ , are given in atoms per ion. Increases in μ with beam energy are a more nearly linear function than has been previously reported in terms of $\mu/1 + \gamma$, where γ is the number of secondary electrons emitted per incident ion. The experimental results are interpreted and analyzed in the light of present theories on sputtering yields and thresholds.

INTRODUCTION

The sputtering or the erosion of surfaces under ion bombardment has long been a subject of interest in atomic physics. Sputtering was first observed by W. R. Grove and reported to the Royal Society of London in 1852[1]. Unfortunately, most investigations carried out since that time are open to doubt because of uncertain experimental conditions. Poor vacuums resulted in contamination of the test surface and unrealistically low sputtering rates were measured. Beams undefined in degree of ionization and energy spread

General Dynamics/Astronautics
ERR-AN-072

led to incorrect interpretations of sputtering results. Measurements were usually made by a cumbersome weighing technique which did not permit detailed investigations of sputtering as a function of beam energy.

With new experimental techniques current investigators are now making reliable measurements.[2,3,4,5] But since these new techniques have only recently come on the scene, most of the interesting experiments are yet to be done. Few of the many target-beam combinations have been investigated. Most measurements are obtained with beams of ions at normal incidence with respect to the plane of the target and little is known of how sputtering varies with angle of incidence. Secondary electron emission during sputtering is not usually taken fully into account and true sputtering rates at high energies are not known. Nothing is known of sputtering by neutral atoms.

Under the support of the Office of Naval Research a sputtering program ~~has been~~ initiated to further the investigation of these unexplored areas employing some of the new advances in experimental techniques[5]. During the first year of the program, the experimental apparatus ~~has been~~ assembled and some results on the sputtering of gold and aluminum in noble gases up to 1000 ev have been obtained.

EXPERIMENTAL METHOD

Sputtering measurements are carried out by bombarding a surface with a beam of ions. A drawing of the ion beam generator is shown in Figure 1. The generator consists of an ion source and focuser[6].

The ion source is patterned after the one described by Finkelstein[7] where magnetically constrained electrons are used to ionize the gas. The

source has a high ionization efficiency and can be operated at chamber pressures of about 2 x 10^{-5} mm of mercury. The energy of the ionizing electron beam can be kept low and doubly-charged ions are not produced. The energy spread of the ions is less than 2 ev. Beams having current densities up to 0.1 ma/cm^2 are produced by the source.

A beam is formed by extracting ions from the ionization chamber and focusing them electrostatically. It then passes into the target chamber where sputtering takes place.

The chamber contains a secondary electron plate, a plated crystal target, and a heater. The energy of the beam is varied by changing the potential of this target.

Early in the studies it was observed that about 1/100 of the ion beam was neutralized as it passed through the focuser due to a charge exchange reaction with the neutral gas background. The energy of these neutral atoms was a few hundred volts, the energy of the ions in the focuser. These energetic neutrals sputtered as much as ions at energies below 50 ev, and introduced uncertainties in the interpretation of ion sputtering results. The neutrals were reduced to low values by electrostatic separation.

Two metal discs which block the line of sight act as separators. By adjusting the focusing potential the ions can be made to stream around the discs. The neutral atoms, unaffected by the focuser, strike the disc and are deflected out of the beam.

ION BEAM GENERATOR

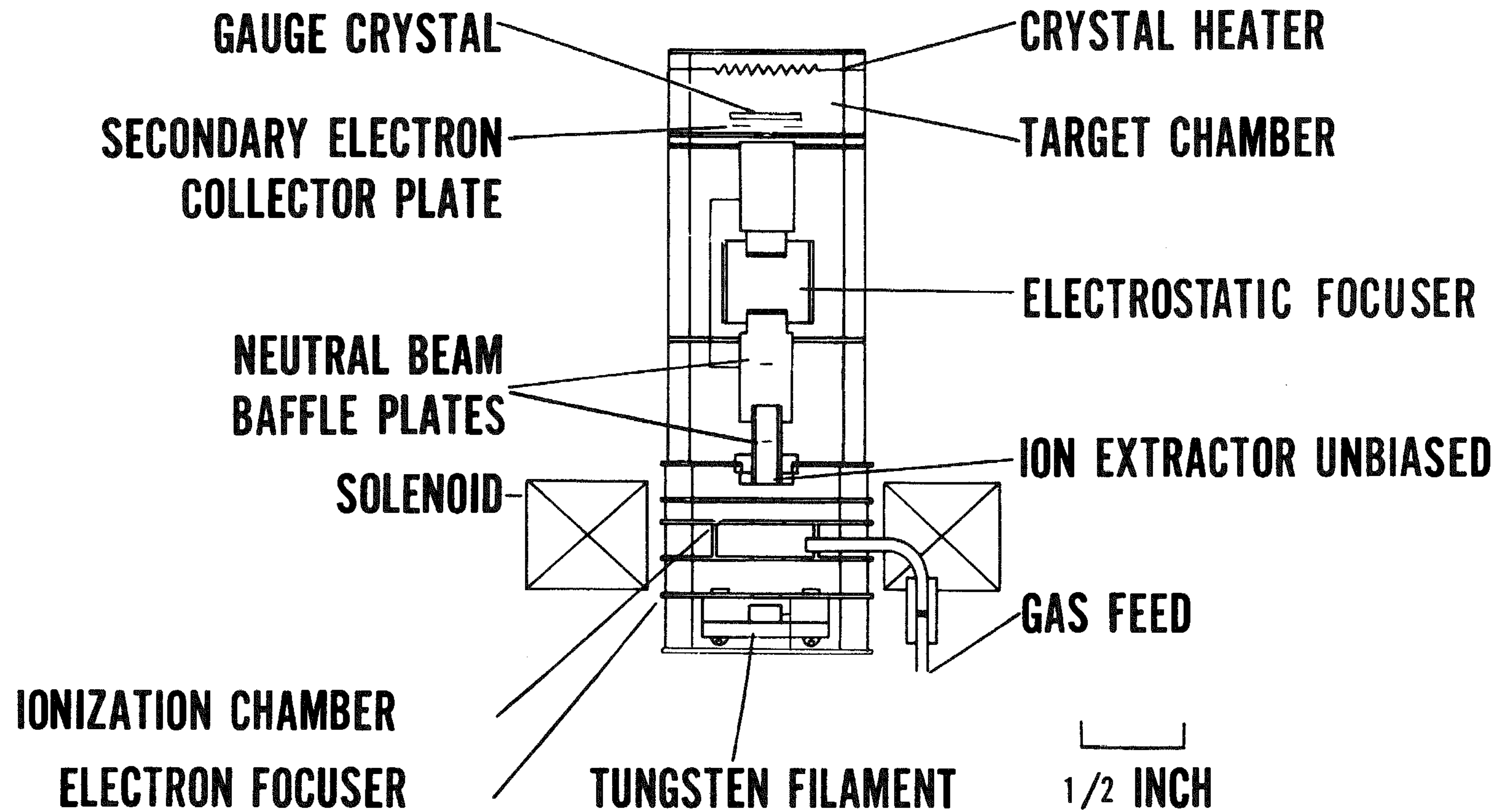

Figure 1

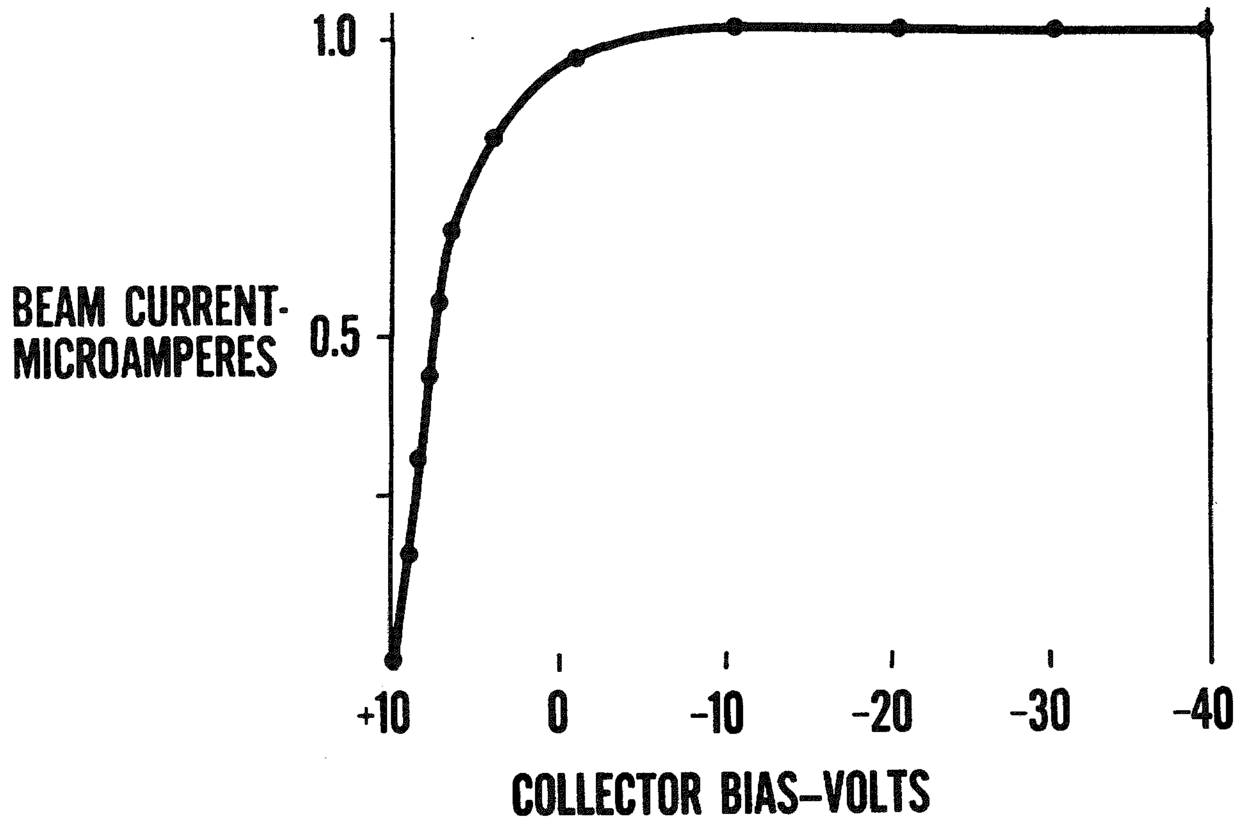

Figure 2

Beam current as a function of target voltage

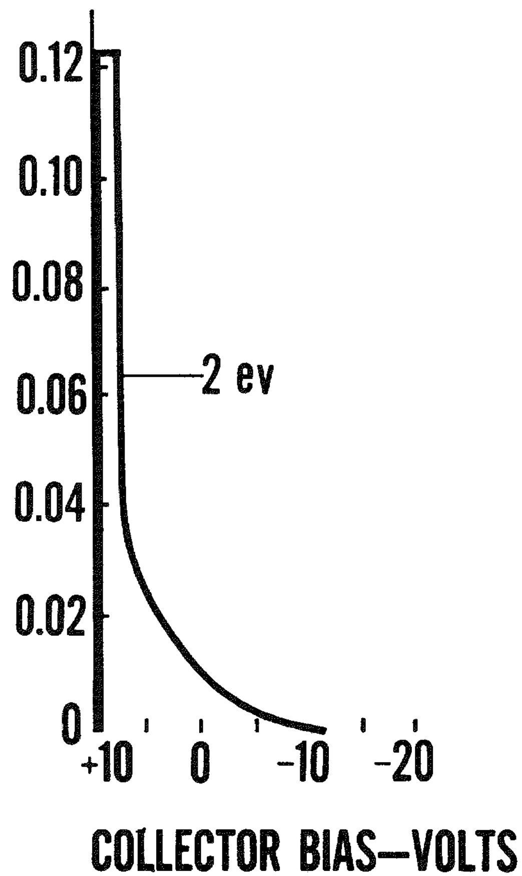

Figure 3

Energy spread of the beam

Figure 2 is a plot of the ion beam current produced by the generator as a function of target voltage. The ionization chamber was biased at 10 volts, the retarding potential necessary to cut off the beam. The energy spread of the beam is found by differentiating this curve and is shown in Figure 3.

Sputtering by an ion beam has several advantages over the more commonly used plasma discharge[8] in which much higher current densities can be obtained. Lower background pressures in the target region can be maintained. The angle of incidence of the beam can be varied. Secondary electron emission measurements can be made. Neutral beams can be generated. The beam can be mass analyzed. For the present experiments with monatomic gases, mass analysis is not employed.

In order to make successful experiments using ion beams with low current densities two requirements must be fulfilled. First an ultra-high vacuum is needed to insure that the test surface remains uncontaminated during the sputtering. Second, a sputtering detector is required having a sensitivity several orders of magnitude greater than the conventional weighing technique. This follows from the fact that the ion current densities of the beam method are several orders of magnitude smaller than the plasma method.

Figure 4 shows the two vacuum chamber systems used in the experiments. The beam generating chamber is a six-inch non-magnetic stainless steel tee commonly used in liquid oxygen transfer lines. It is fitted with internal bake-out heaters and is evacuated by a 400 liter/sec mercury pumping system to pressures of 10^{-8} mm of mercury. Mounted on the top face plate is an 8 liter/sec VacIon pump used for evacuating the target chamber.

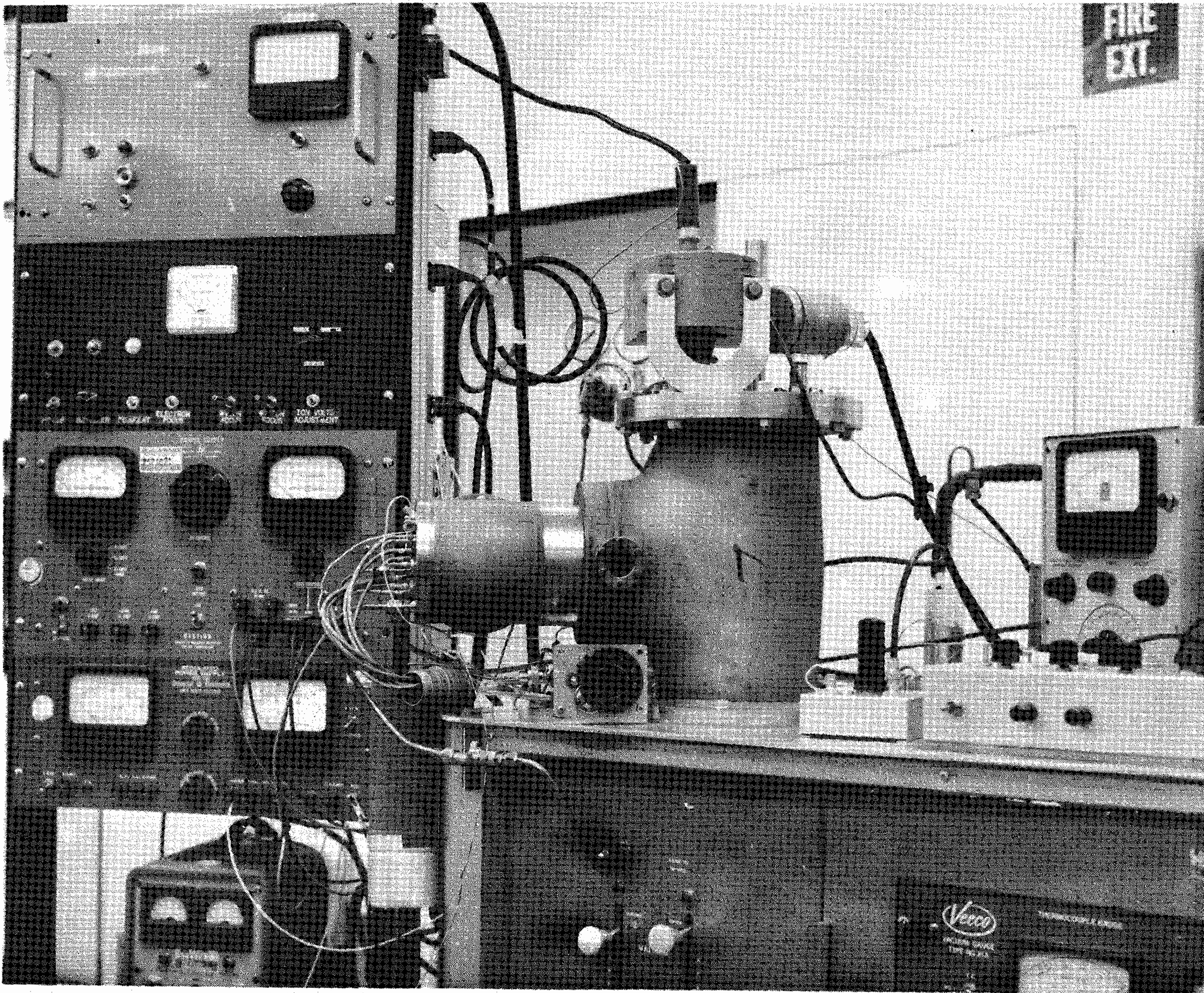

Figure 4

Experimental Apparatus

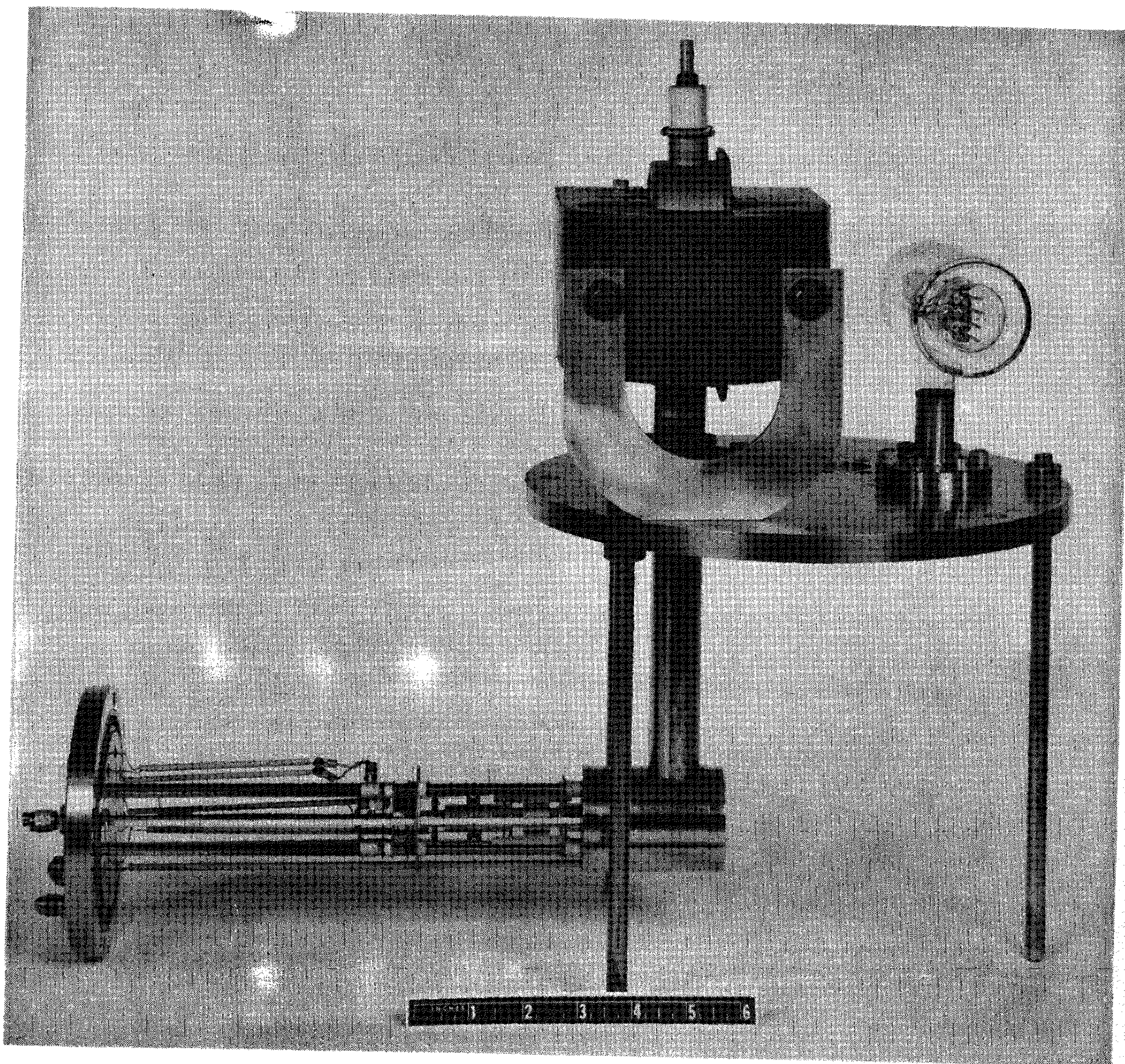

Figure 5

Beam generator

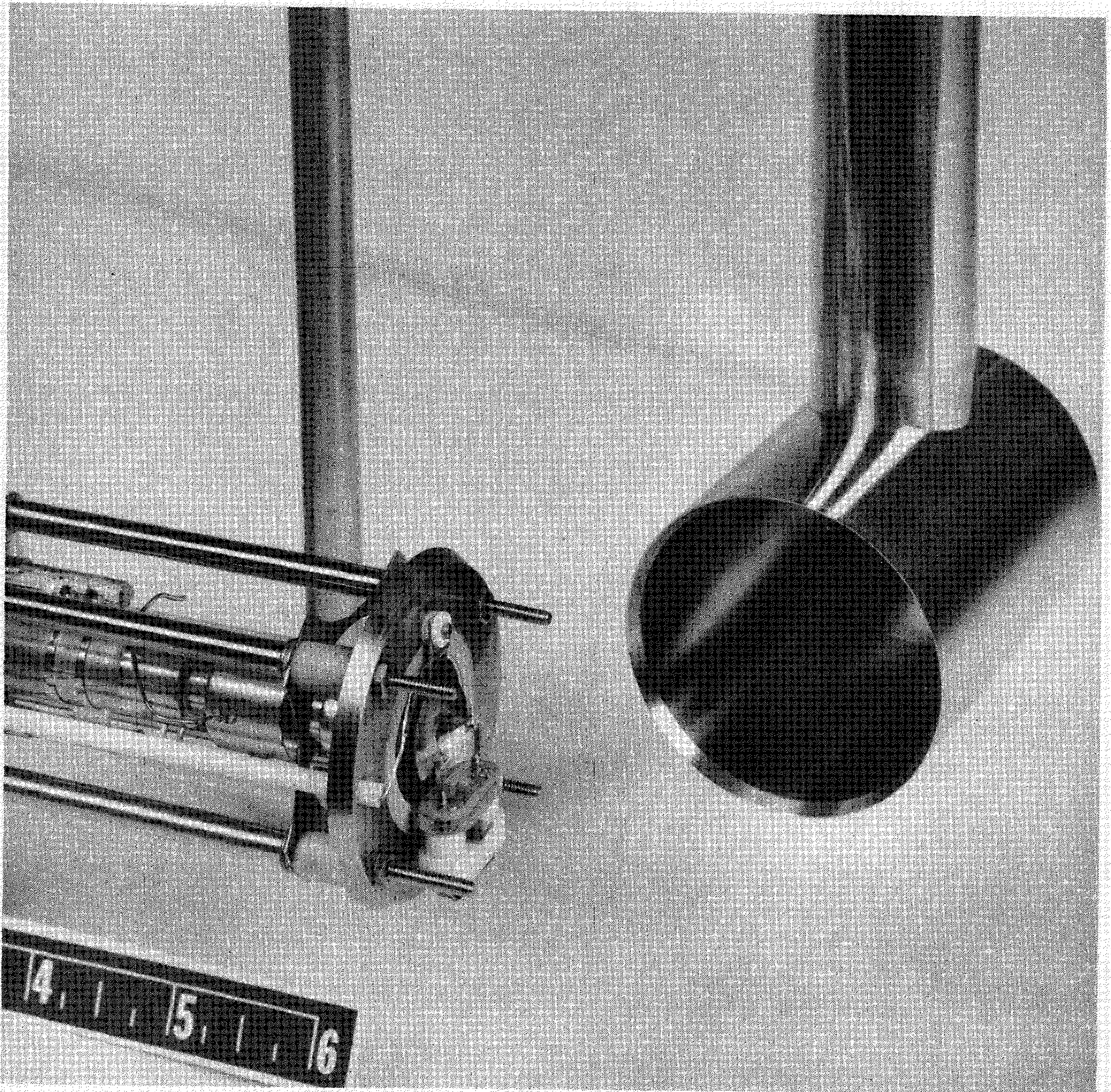

Figure 6

Target chamber

Figure 5 is a photograph of the beam generating chamber, showing the location of the beam generator and the internal target chamber with its Vac-Ion pumping line. The target chamber is pumped to pressures of 10^{-9}mm of mercury.

Figure 6 is a close-up of the beam generator with the chamber removed. Exposed are the graphite baffle plate, secondary electron collector and target crystal.

Sputtering was measured by the crystal oscillator method[5]. Figure 7 shows a 10-Mc crystal resonator typical of those used. It is a precision, optically polished quartz crystal whose frequency varies less than 0.000001 cycle/^{o}C. Crystals were cut to operate at 60°C and controlled to 0.01^{o}C by an oven.

The material to be studied is plated on the crystal approximately 2000 - 5000Å thick. The crystal is bombarded by the beam and sputtering of its plating is measured directly by the resonance frequency change of the crystal. 20-Mc crystals whose frequency increased one cycle per 1.5×10^{-10}gm sputtered were employed for measurements in the threshold region. 10-Mc crystals which are one-fourth as sensitive as the 20-Mc ones were employed for measurements at high sputtering rates above the threshold region. Although the 10-Mc crystals are less sensitive, they will take a heavier plating and have a longer sputtering life. The same crystal can be used to run curves on several gases. In general, the lower the resonance frequency the thicker the plating. The crystal oscillator method can then be used on high sputtering rate experiments by a proper choice of frequency.

10-MC CRYSTAL RESONATOR

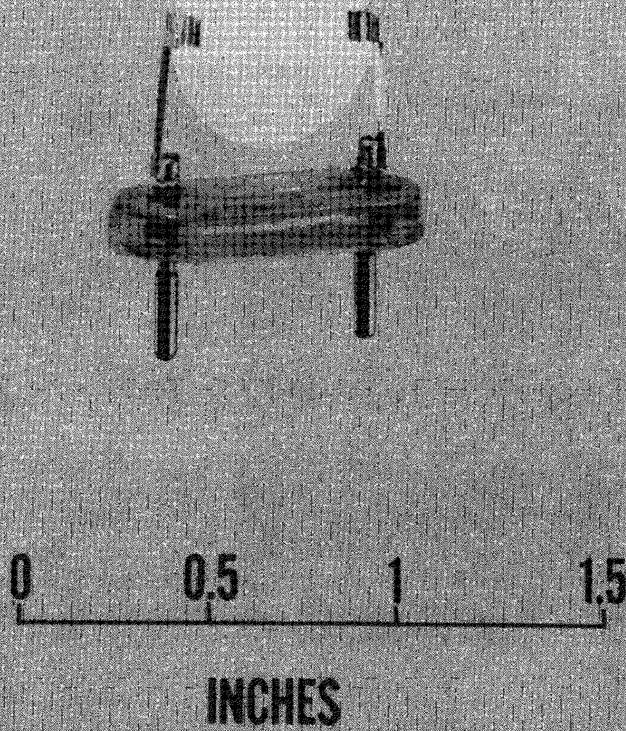

Figure 7

Figure 8

Evaporator unit for plating quartz crystals

The calibration of the frequency change of the crystal in terms of mass sputtered can be accomplished in several ways. It can be done directly by measuring film thickness. A partially plated oscillating crystal and an optical flat are placed side by side in a vacuum evaporator. Both are plated with about 2000Å of the required material. The decrease in crystal frequency is observed. The amount of material plated on the crystal is determined from analyses of the optical flat by the interference fringe method described in detail by Tolanksy[9].

Figure 8 shows the evaporator unit in operation. The oscillator for driving the crystal is mounted on the top face plate. A Hewlett-Packard Model 524C counter is used for monitoring the frequency of the crystal.

Another direct way is by sputtering calibration. The sputtering rate of a block of test material is measured in an ion beam by weight loss. Once the sputtering rate is known in atoms per ion, the frequency mass relationship of a crystal plated with the same material can easily be found by sputtering it under the same ion beam conditions.

The simplest method is to calculate the frequency mass relationship from the fundamental frequency of the crystal. This way agrees within 10% with the more laborious direct methods, as long as at least 50% of the crystal plating is uniformly eroded during sputtering.

An energized crystal is a mechanical vibrating plate which is coupled to the driving oscillator by the piezoelectric effect. Its electronic frequency is dependent on its equivalent electrical parameters[10]. The parameter of importance in determining the mass sputtered is the equivalent

inductance which is dependent on the resonating mass of the plated crystal. Equation 1 expresses the frequency in cycles per second, in terms of the crystal thickness[11], t, in millimeters. Using the equation one can compute the frequency change Δf, produced by a removal of a thickness, Δt, of the plating.

A thin plating behaves like an equal mass of quartz. The constant, k, is characteristic of quartz and is independent of the plating.

1. $f = k/t$ where k equals 1.66×10^6 cycles-mm/sec

2. $\Delta f = -k \quad \Delta t/t^2$

Using a precision 10-Mc crystal, the plating thickness removed for a measureable 1 cycle increase in frequency is the following:

3. $\Delta t = -k \quad \Delta f/f^2 = -1.66 \times 10^{-8}$ mm = -.166 angstrom

Since Δt is inversely proportional to f^2, a higher fundamental frequency would give even greater sensitivity. For example, using a 20-Mc crystal an average change in thickness of only 0.04 angstrom units of quartz could be measured.

The sensitivity of the crystal to erosion increases with the atomic weight of the plating. For example, a gold plated crystal is sensitive to the removal of only 0.01 Å.

Using a crystal with a 4 mm plating diameter the following decrease in plating mass Δm, can be measured.

4. $\Delta m = \rho A \Delta t$

$\Delta m = -5.5 \times 10^{-10}$ gram

where ρ is the density of quartz, 2.6 gm/cm^3

It should be noted from equations (2) and (4) that an equal mass deposited on the crystal would produce a corresponding frequency decrease. Hence, it is obvious that the evaporative overplate method is possible for crystal calibration.

The maximum plating thickness to which a crystal can be plated has been discussed in detail in previous work[10]. The effect of the plating thickness appears as part of the motional resistance in a resonating crystal. Figure 9 is the equivalent electrical circuit of a crystal.

Figure 10 is an admittance plot of the motional inductance, capacitance, and resistance. On the curve-linear coordinates of a Smith chart the admittance plot is a circle. At resonance the capacitive reactance cancels the inductive reactance and the diameter of the circle is the reciprocal of the motional resistance.

The motional resistance is a measure of the vibration loss of a crystal plus the loading effect of the plating. For optimum plating thickness the loading should be less than 1/10 of the motional resistance. Experimentally, the maximum plating thickness is found to fall between 3000 to 5000 Å for 10 to 20-Mc crystals.

CRYSTAL EQUIVALENT ELECTRICAL CIRCUIT

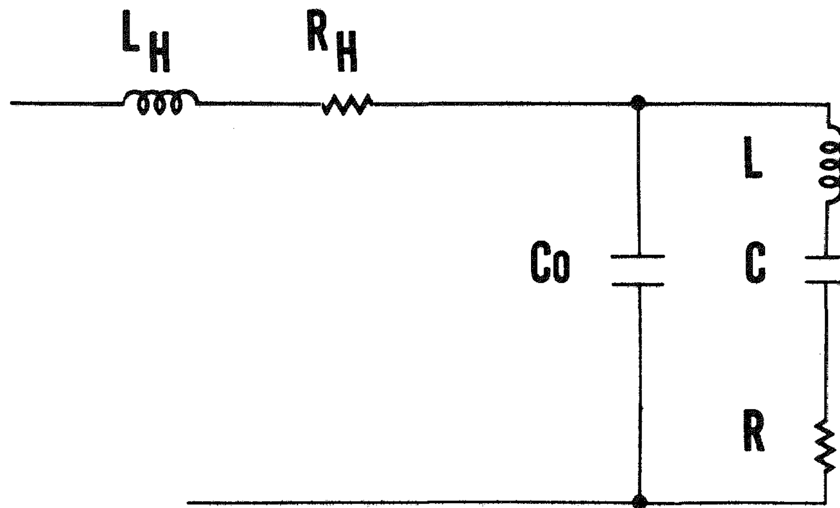

L_H - HOLDER INDUCTANCE

R_H - HOLDER RESISTANCE

Co - PLATING CAPACITANCE

L - MOTIONAL INDUCTANCE

C - MOTIONAL CAPACITANCE

R - MOTIONAL RESISTANCE

Figure 9

EQUIVALENT CIRCUIT ADMITTANCE PLOT

DIA. OF CIRCLE DECREASES AS PLATING IS INCREASED

ADMITTANCE CIRCLE FOR OPTIMUM PLATING THICKNESS

RADIALLY SCALED PARAMETERS

TOWARD GENERATOR

TOWARD LOAD

CENTER

Figure 10

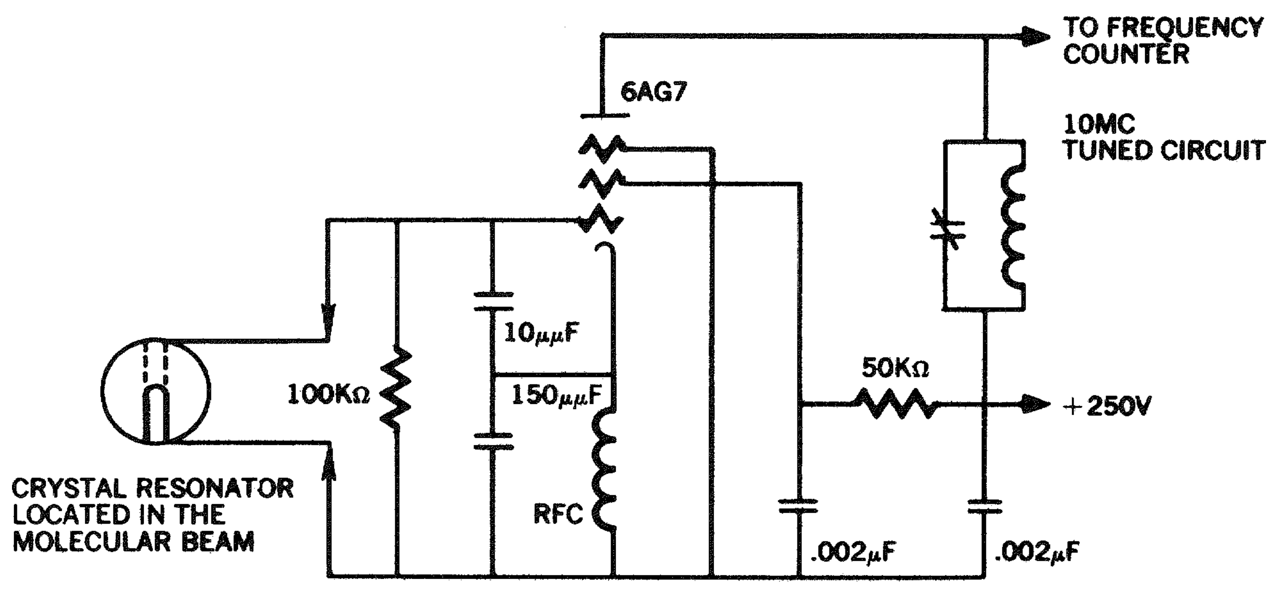

Figure 11

10-Mc crystal oscillator

The oscillator circuit used for driving 10-Mc crystals is shown in Figure 10. For 20-Mc crystals the tank circuit is tuned to 20-Mc. The frequency is measured with a Model 524C Hewlett Packard counter and is recorded with a Model 560A digital readout.

EXPERIMENTAL RESULTS

Experimental data was obtained by measuring the change in frequency of the crystal as a function of the bombarding energy of the beam. Figure 12 shows some typical results obtained with a 20-Mc crystal. The high sensitivity of the resonance frequency of a crystal to mass sputtered allowed individual data points to be taken at 30-second intervals. The accuracy in making the measurements was limited to 20% due mainly to crystal calibration and neutral beam sputtering variations.

Sputtering rates in atoms per ion were determined from the following equation where, Δf is the frequency change of the crystal in cycles per second, N is Avogadro's number, F is the mass frequency constant of the crystal, M is the gram atomic weight of the plating material, I is the beam current in ions per second, and T is the period of bombardment in sec.

5. $$\mu = NF\,\Delta f/M_p IT$$

Where $F = 5.5 \times 10^{-10}$ gram/cycle for a 10-Mc crystal

$F = 1.4 \times 10^{-10}$ gram/cycle for a 20-Mc crystal

The ion beam current bombarding the crystal targets was measured by a Keithly Model 610 electrometer. Secondary electrons were suppressed by keeping the bias of the secondary electron collector and baffle plate (See Figure 1) at 200 volts above the target potential.

Attempts to accurately measure the flux of secondary electrons produced by ion bombardment during sputtering were thwarted by electrons present in the target region arising from other interactions. The main source of these electrons was the collision of ions with neutral gas atoms at 2×10^{-5} mm of mercury in the focuser. The beam generator is now being modified to measure only secondary electrons under conditions described by Hagstrum[12] where background pressures are less than 1×10^{-8} mm of mercury.

Runs were made with different beam currents to show that the sputtering rates were independent of current, (See Figure 12). For example, at 60 ev, after subtracting out the neutral sputtering background, both the 1 and 3 microampere beams have a yield of 60 cps per min per sec microamp. The fact that the sputtering rate is independent of bombarding current shows that the test surface remained clean during the measurements. Although electrostatic separation was employed, it was not possible to completely reduce the neutral beam since a small fraction was formed in the distance between the separator and the target.

Results for the sputtering of gold in He^+, Ne^+, Ar^+, and Xe^+ for energies below 100 ev at normal incidence are shown in Figure 13. Rates are plotted on a log scale to conveniently cover the range of 10^{-3} to 1 atom/ion. Although the crystal oscillator method is sensitive enough to measure down to 10^{-6}, sputtering due to neutral atoms leads to an uncertainty in the interpretation of the data below 10^{-3} and are not given.

Results for the sputtering of gold at energies above 100 ev at normal incidence are shown in Figure 14.

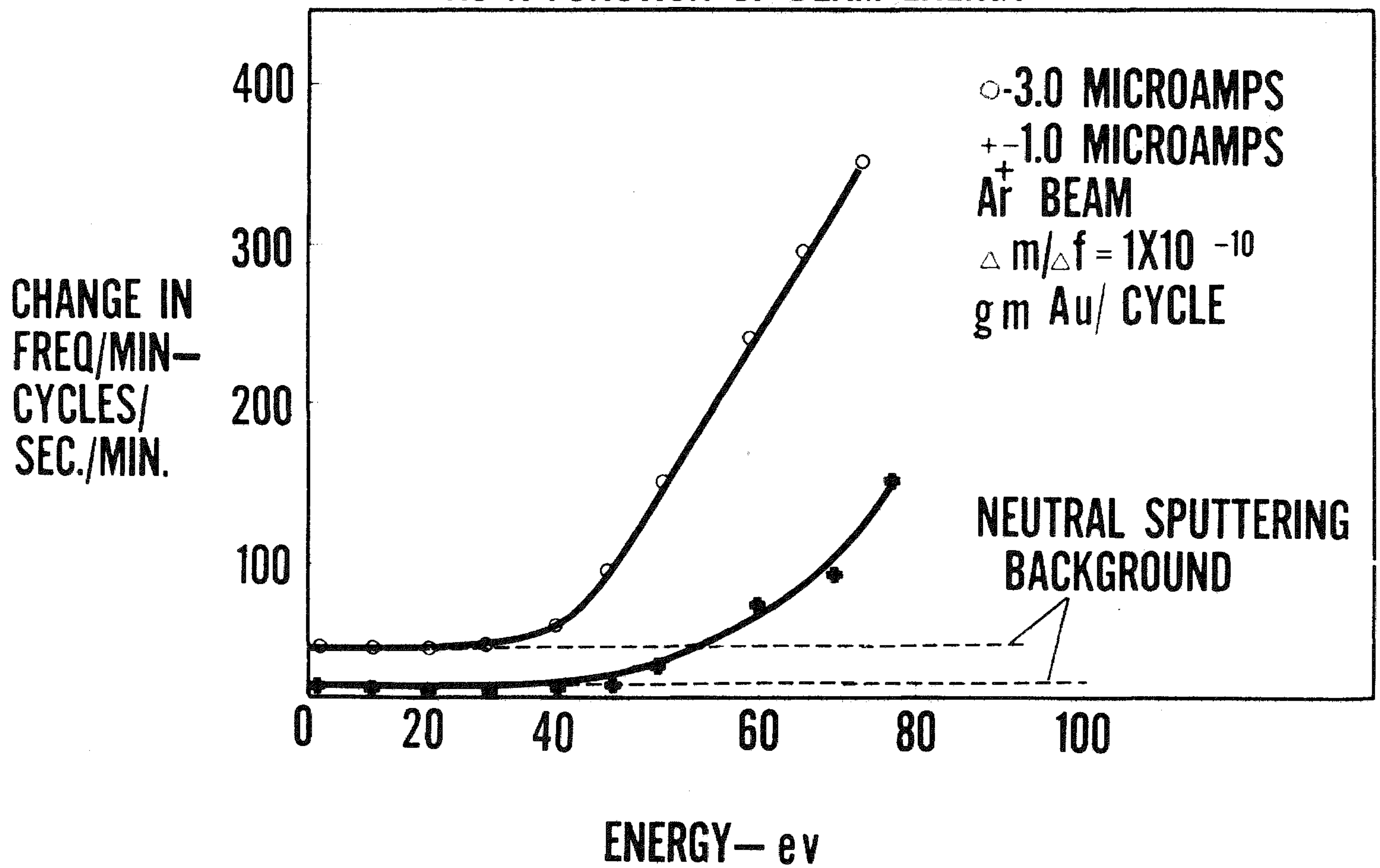

Figure 12

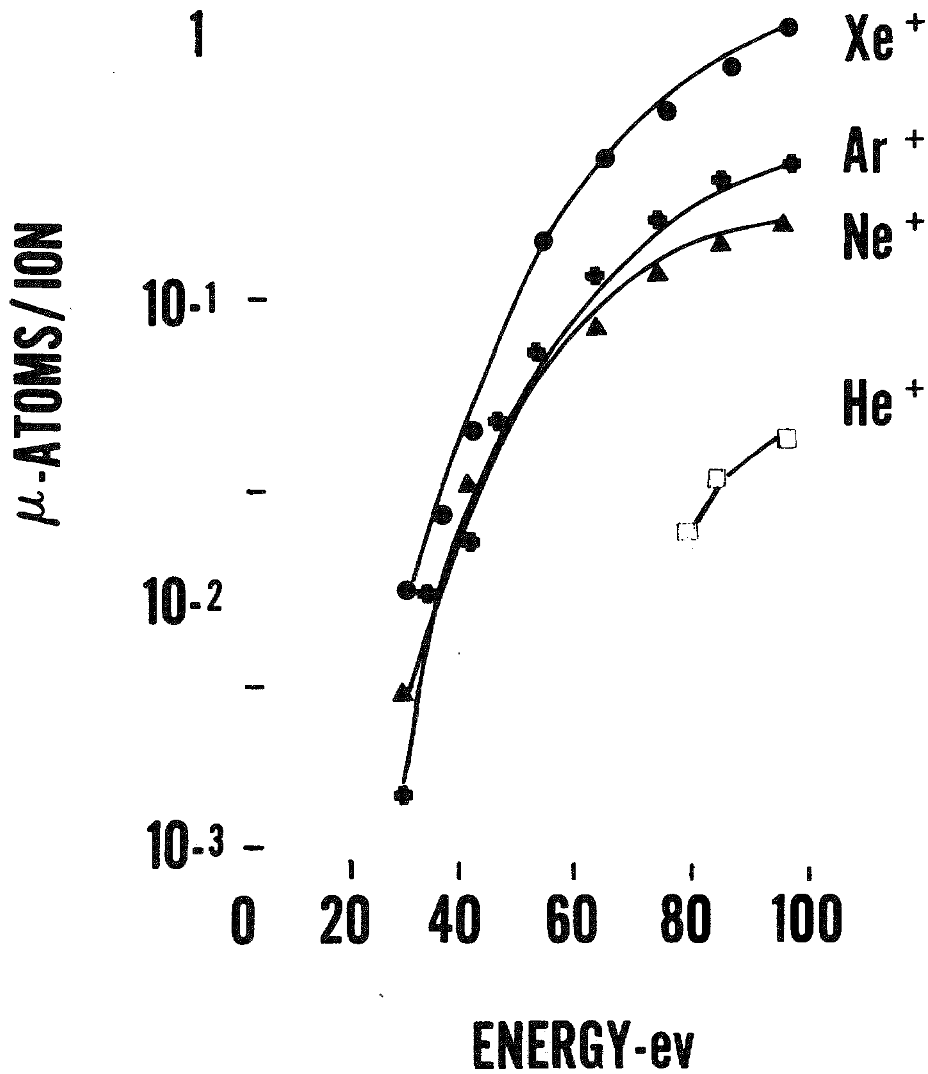

Figure 13

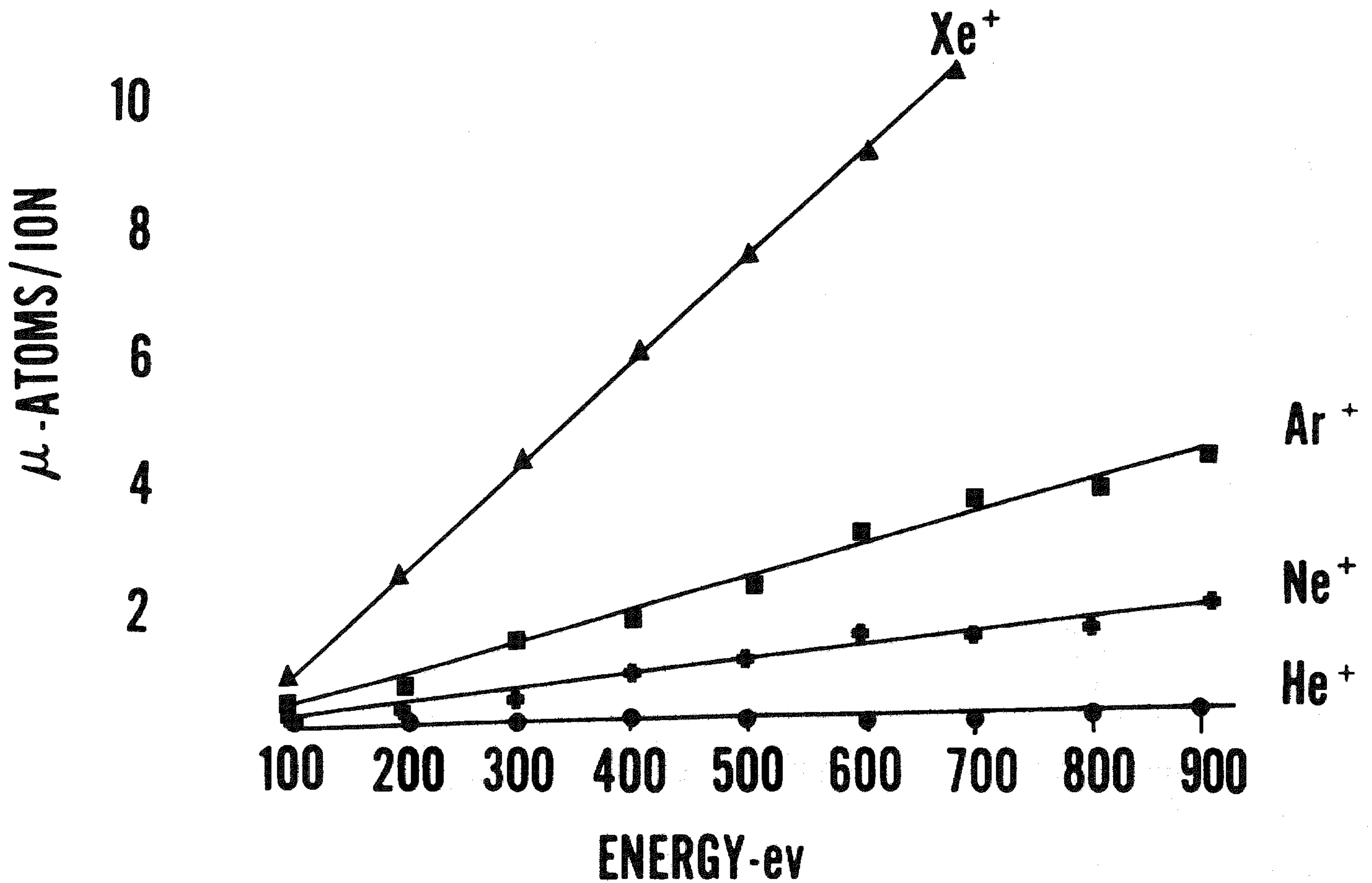

Figure 14

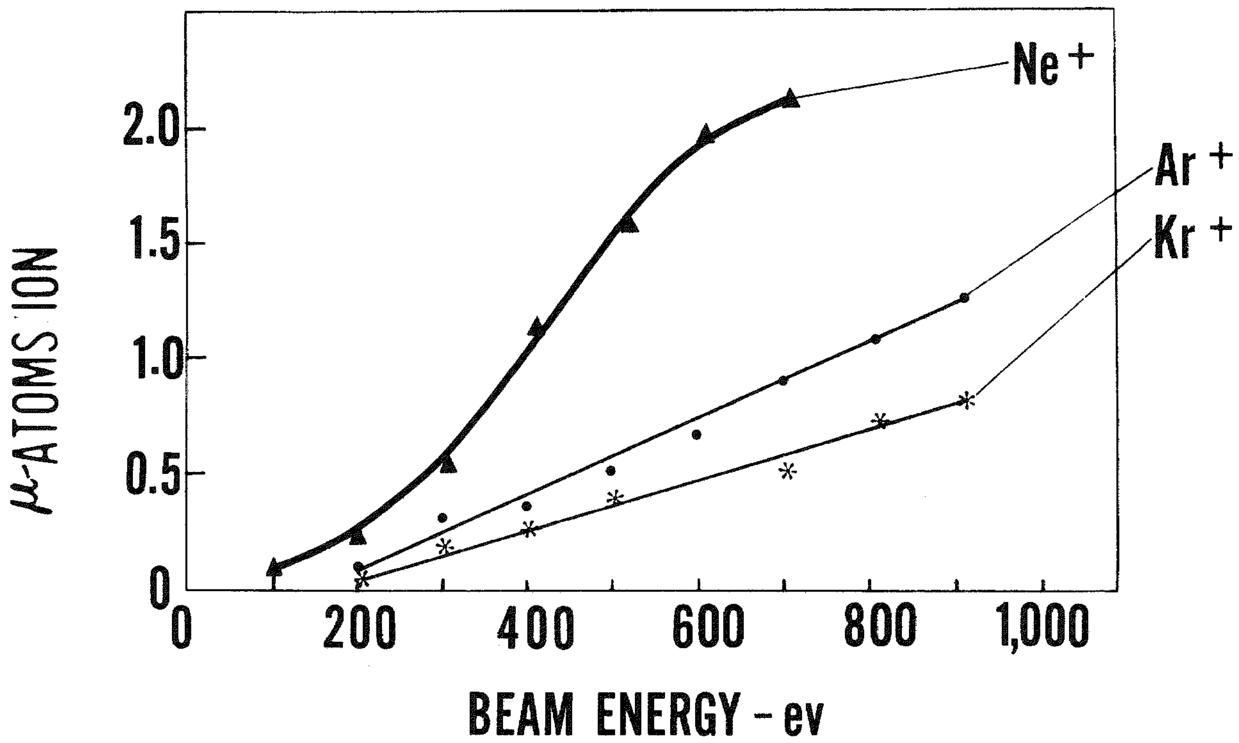

Figure 15

Results for the sputtering of aluminum at normal incidence by Ne^+, Ar^+, and Kr^+ at energies between 100 and 1000 ev are shown in Figure 15. It was not possible to continue the measurements below 100 ev because of the extremely low sputtering rates. The reaction of aluminum with both He and Xe contaminated the surface and prevented any good measurements.

COMPARISON WITH OTHER RELATED EXPERIMENTS

Only Wehner and his group have published recent results[13,14] for gold and aluminum in noble gases, and these are for neon and argon. Unfortunately, Wehner's results cannot be compared directly with those given here because his measurements give $\mu/1+\gamma$ instead of the true sputtering rate μ. γ is the number of secondary electrons ejected per incident ion. If γ is comparable to one, $\mu/1+\gamma$ is significantly less than μ.

Figure 16 shows a comparison of the measurements of gold in Ne^+ and Ar^+ and aluminum in Ne^+. At low energies the comparison is good, but at energies about 200 ev the sputtering rates in terms of $\mu/1+\gamma$ fall off. This is attributed to high secondary electron emission at these energies.

Figure 17 brings out more fully the effect of secondary electron emission on the character of sputtering rate measurements at high energies. Wehner's results[13] for molybdenum are shown corrected for γ from data given by Hagstrum[15]. This indicates that the sputtering rates between about 100 and 1000 ev are more linear in energy than was previously inferred from $\mu/1+\gamma$ measurements.

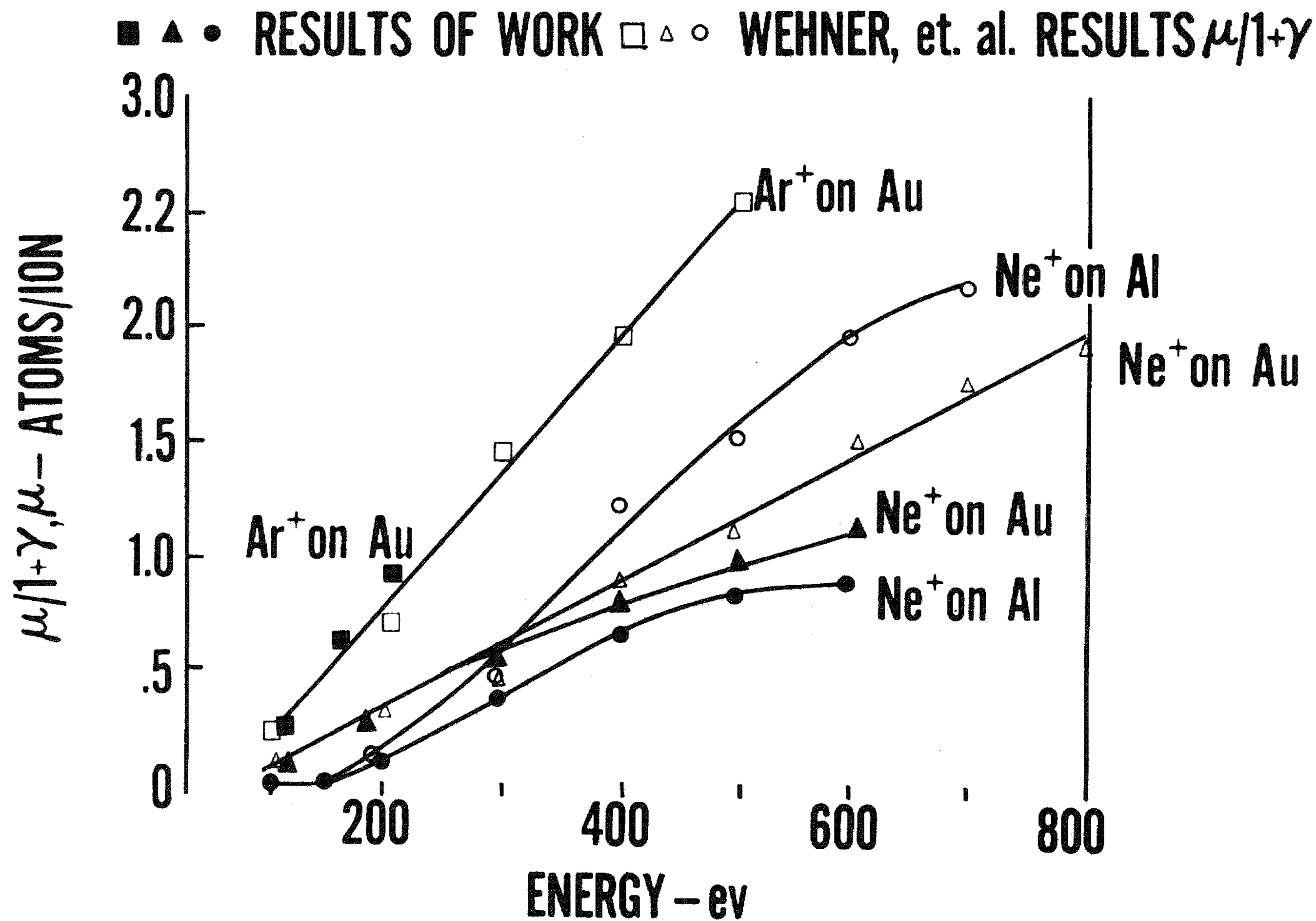

Figure 16

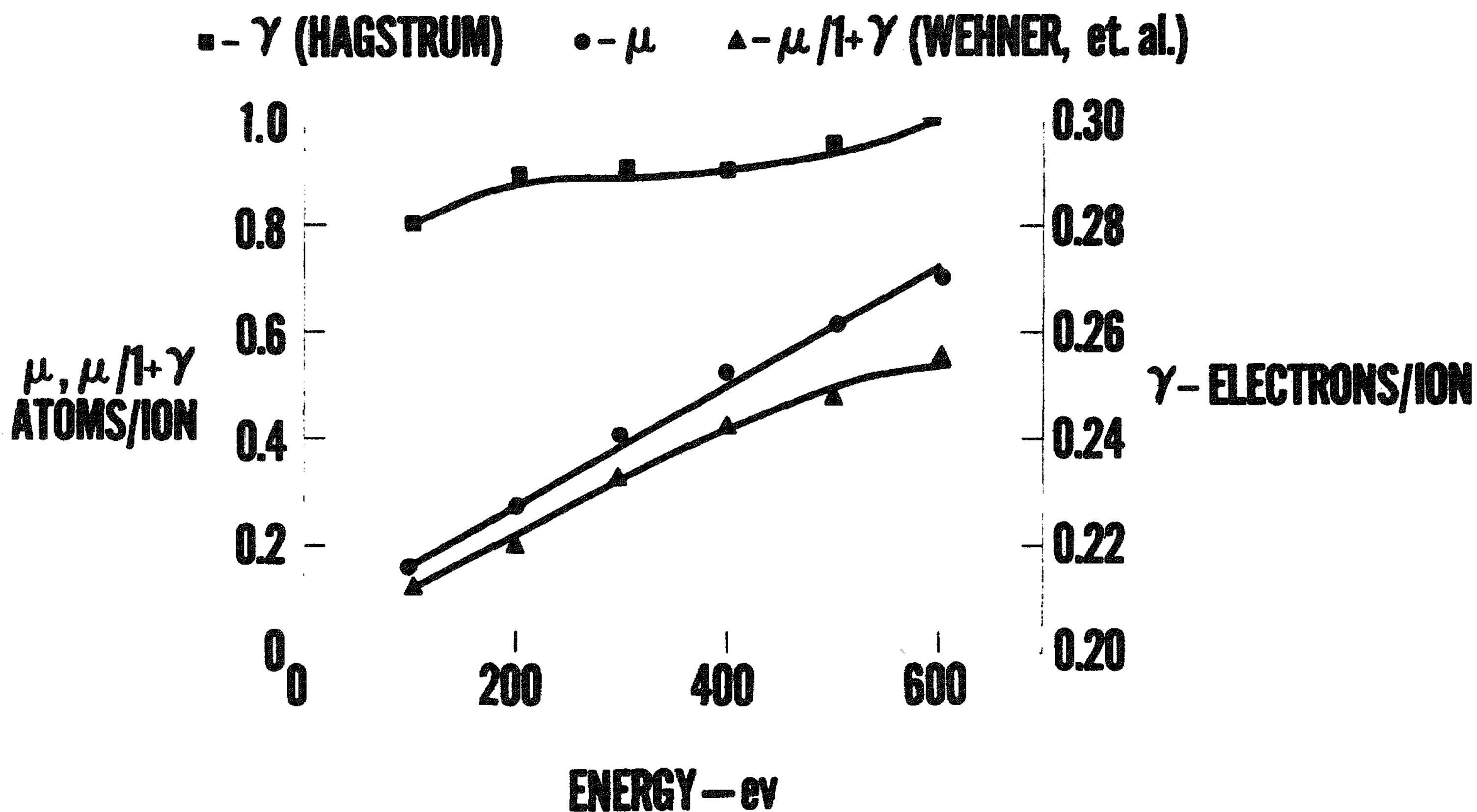

Figure 17

No measurements have been found in the literature to compare with results given here for gold below 50 ev (Figure 13). But the sharp drop in yield below 50 ev substantiates the results of Wehner for other metals at low energies.

DISCUSSION OF SPUTTERING THEORIES

One of the goals of the low-energy sputtering studies is to measure the "threshold of sputtering." Threshold is defined here as that energy below which no significant sputtering occurs. From the measurements of gold, Figure 13, the threshold occurs between 20 and 30 ev. It is necessary to define the threshold in this way because there are always a few loosely bound atoms on a surface which could be sputtered if given a "slight nudge." But these atoms are so exceptional that their ejection has no more significant effect on the properties of a metallic surface than those that leave due to vapor pressure.

A number of recent theories have been proposed to define sputtering in the threshold region[16,17,18,19,20]. They treat the interaction between the bombarding ion and target atom as a hard sphere collision. For normal incidence the bombarding ion undergoes at least one collision to reverse its momentum vector before a second collision can produce sputtering. The bombarding ion strikes a target atom and rebounds in such a direction as to sputter another atom from the surface. The other possibility is that the bombarding ion displaces from its site the first atom it meets and is subsequently lost in the interstitial spaces of the lattice. Meanwhile, the

displaced atom uses up its excess kinetic energy to collide with other atoms in the lattice. A certain percent of the time, this atom will strike an atom near the surface with enough energy to cause sputtering. At oblique incidence a single collision can lead to the ejection of a surface atom.

To calculate the threshold energy, E_t, the angle of incidence is assumed, the equations for the conservation of energy and momentum are taken into account and the following other parameters are considered: the mass (m) of the impinging ion, the mass (M) of the target atom, the average binding energy of an atom in the lattice, the crystal structure of the metal, the heats of sublimation of the different crystal planes, the collision radii of the target atoms, and the energy dissipated in the lattice as heat. Henschke points out the dependence of the theoretical E_t on the collision radii. This dependence reveals a marked periodicity of this energy as a function of the atomic number of the target atom. More specifically, this behavior is seen to be related to the filling of the d subshells, (electronic orbital angular momentum $\ell = 2$) in the electronic structure of the elements. It is observed that for these atoms with nearly completely filled d shells, the collisions are more elastic and less energy is lost in the lattice. This results in higher sputtering yields for these metals.

ANALYSIS OF RESULTS

The data given on Figure 13 for the sputtering of gold fits best the theories given by Henschke and Langberg. These theories were based on experimental results of Wehner using mercury beams to bombard various surfaces

at normal incidence. Sputtering yields in the threshold region follow parabolas of the form

$$6. \quad \mu = \alpha_1 (E - E_t)^2 + \alpha_2 \qquad \text{for } E_t < E < E_p$$

where E is the energy of the bombarding ion, E_t the threshold energy, and α_1 and α_2 are constants.

Langberg has given a formula which takes into account the linear behavior of sputtering as shown in Figure 14.

$$7. \quad \mu = 2\alpha_1 (E_p - E_t) \left\{ E - \tfrac{1}{2} (E_p + E_t) \right\} \qquad \text{for } E_p < E < E_e$$

The constant α_1 is the same parameter which was obtained from a calculated fit of the low sputtering in the "parabolic region". Also, one obtains E_t and E_p from measurements in this region. Note that α_2 is usually so small that it may be neglected in this region of sputtering. As a result there is a degree of consistency in the formulation since it is possible to use the same set of parameters to fit both the linear and parabolic sections of the yield curves.

Figure 18 is a schematic yield curve indicating the characteristic behavior of the effect in this energy range. Also the critical energies E_t, E_p, and E_e are marked on the curve. E_t is the usual approximate threshold energy, E_p is that energy at which the parabolic nature of the sputtering curve ends, and E_e is the energy at which the linear nature of the curve ceases. After E_e, the yield starts leveling off to some value at the higher

SCHEMATIC YIELD CURVE
VARIOUS BOMBARDING BEAM ENERGIES

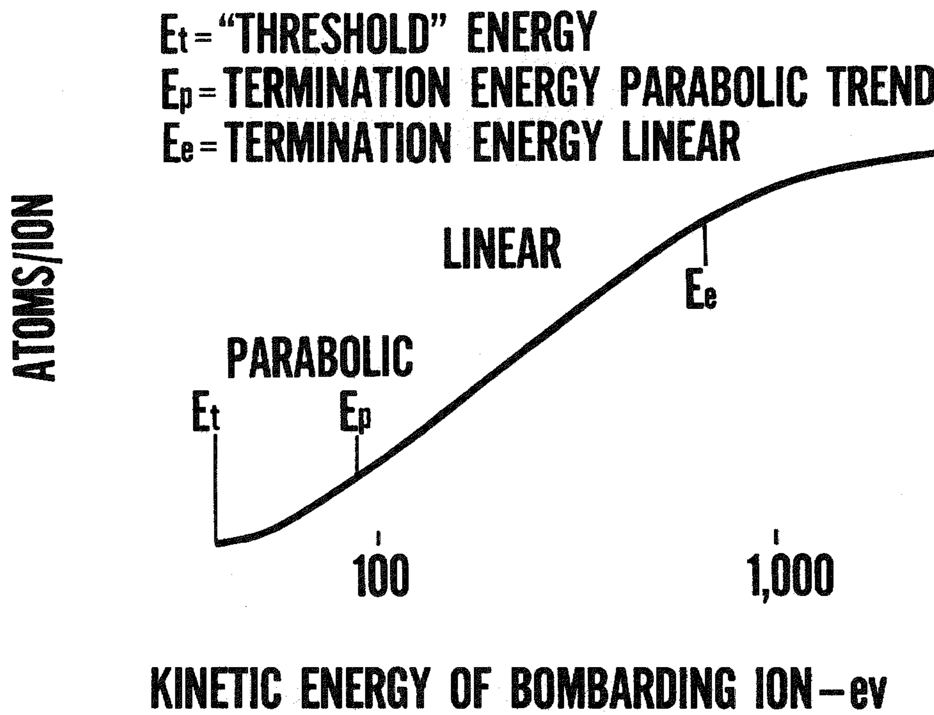

Figure 18

energies.

Using the data on Figures 13 and 14 to solve for the constants in equation (7) the sputtering curves of gold can be fitted by the following equations:

For He^+,

$$\mu = 4.0 \times 10^{-5} (E - 70)^2 + 9 \times 10^{-3} + 4.0 \times 10^{-4} (E - 72)$$

For Ne^+,

$$\mu = 5.5 \times 10^{-5} (E - 30)^2 + 2.75 \times 10^{-3} (E - 42)$$

For Ar^+,

$$\mu = 8.0 \times 10^{-5} (E - 35)^2 + 7.2 \times 10^{-3} (E - 57)$$

For Xe^+,

$$\mu = 15.0 \times 10^{-5} (E - 25)^2 - 3 \times 10^{-2} + 1.86 \times 10^{-2} (E - 56)$$

Since the measurements for aluminum are not complete no attempt was made to fit any curves to it. An important parameter which can be applied to the aluminum data as well as that for gold is the energy transfer coefficient.

The energy transfer coefficient, $\eta = 4mM/(m + M)^2$, arises from the energy and momentum conservation equations[13]. The theoretical formula for E_t by Henschke shows E_t directly proportional to this factor for both normal

ENERGY TRANSFER COEFFICIENT
GOLD & ALUMINUM

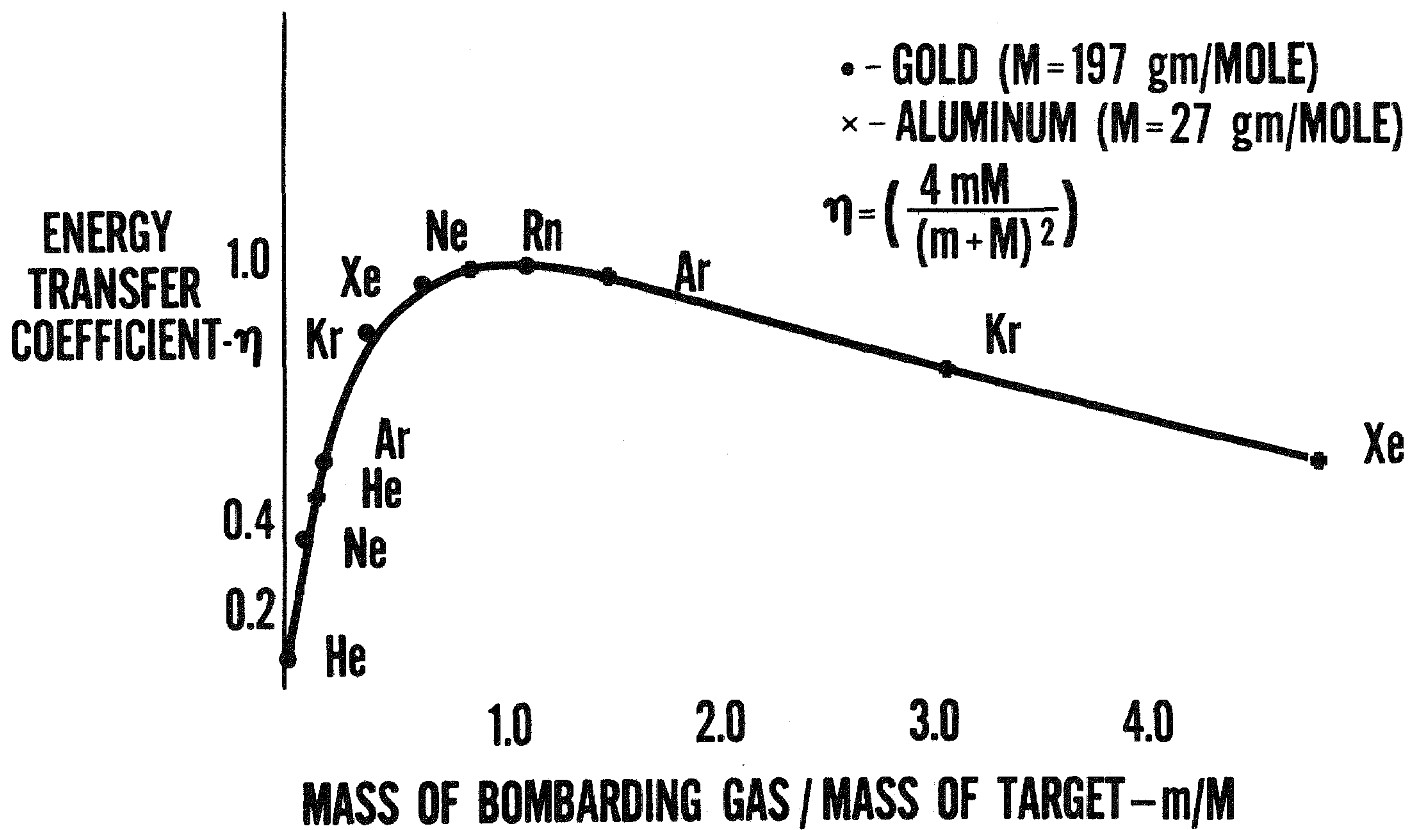

Figure 19

SPUTTERING YIELD OF GOLD
AS A FUNCTION OF ATOMIC WEIGHT OF BOMBARDING GAS

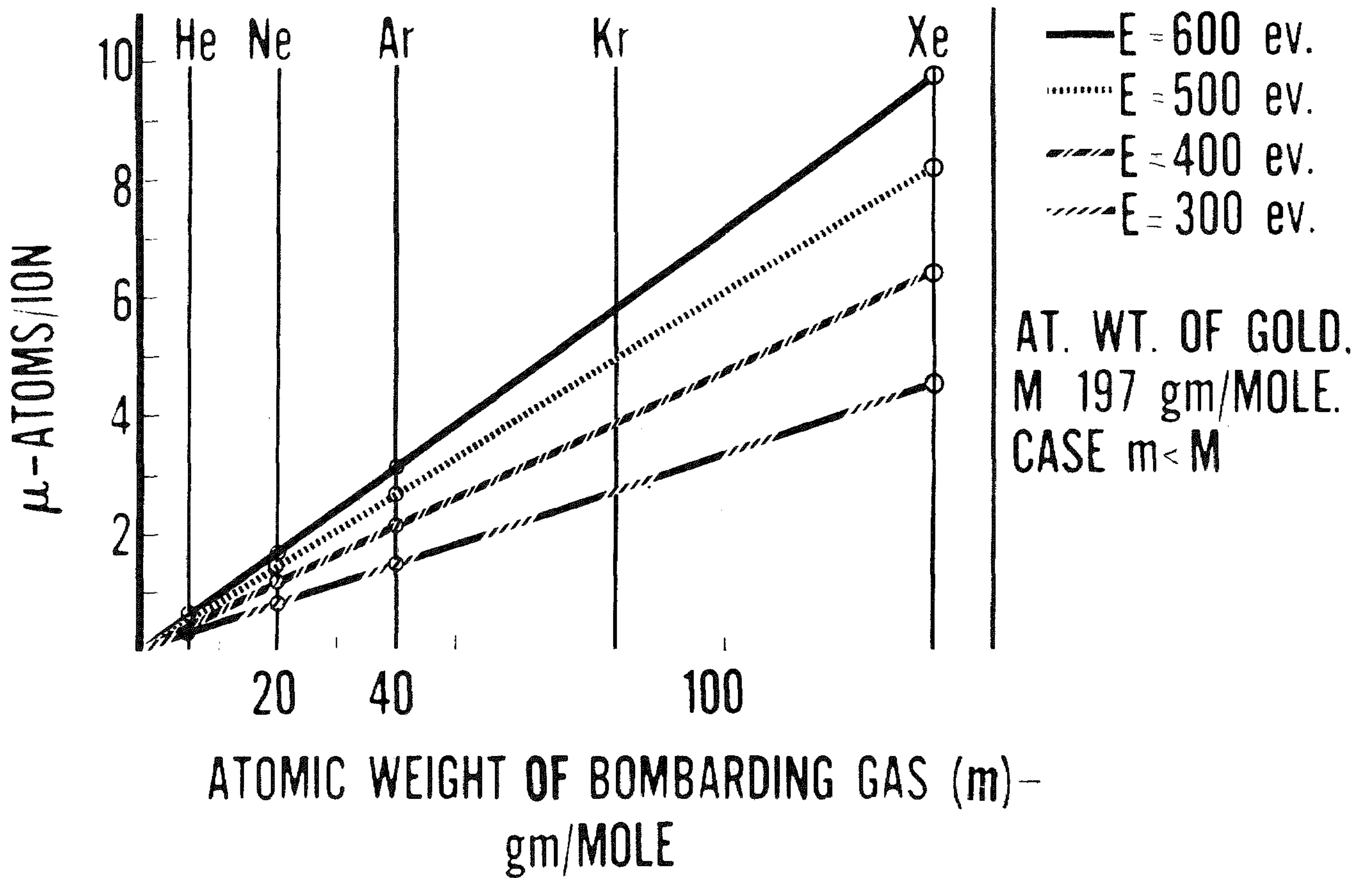

Figure 20

SPUTTERING YIELD OF ALUMINUM
AS A FUNCTION OF ATOMIC WEIGHT OF BOMBARDING GAS

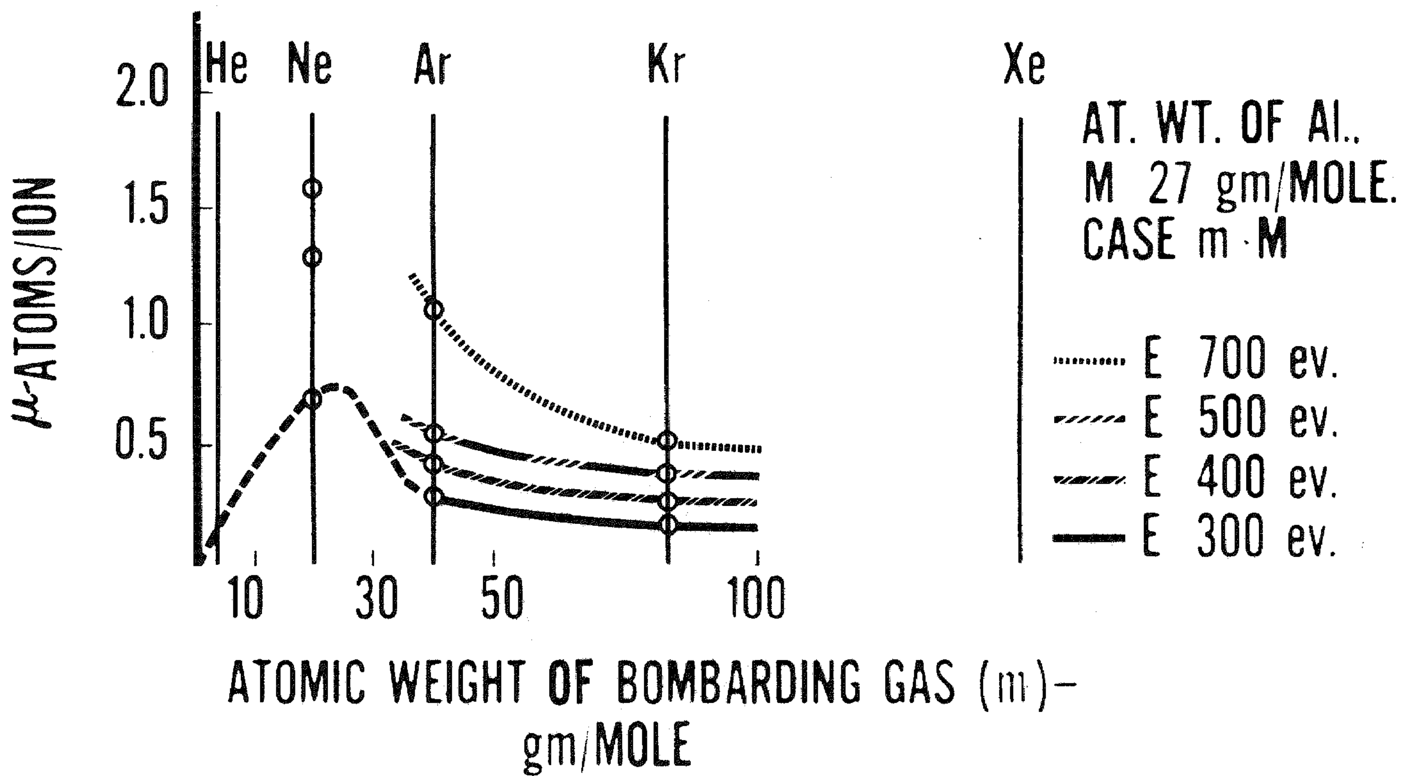

Figure 21

and oblique ion incidence. If one assumes that the collisions at the very low energies are of the one or two-body types, the yield curve would be expected to depend qualitatively on the inverse of η. Figure 19 shows η as a function of m/M. Based on the energy transfer coefficient the sputtering rates of gold should increase from He through Xe. Figures 13 and 14 show this to be the case. For aluminum, the sputtering should be a maximum for Ne with Ar and Kr about equal. Figure 15 shows this to be true. It is apparent that η also has a strong influence on sputtering above 100 ev (Figures 13 and 14) where multiple collisions occur.

It is also interesting to analyze the yield versus energy curves, Figures 14 and 15, by plotting the yield of the metal, μ, at a constant bombarding energy, as a function of the atomic weights of the different bombarding atoms, m. For the case $m < M$, where M is the atomic weight of the target atom, μ increases linearly with m. This is illustrated in Figure 20 for the case of gold.

For the other case $m > M$, which is true for argon and krypton on aluminum, μ decreases with m. This is shown in Figure 21. As m approaches M, μ reaches a maximum. The exact nature of the variation of μ with m, M, and E requires more measurements and is shown diagrammatically by the dashed line in Figure 21.

ACKNOWLEDGEMENTS

The authors are grateful for the support of this program by the Office of Naval Research. They also wish to acknowledge the assistance of many of the members of the Space Physics Group needed in the completion of this work.

BIBLIOGRAPHY

1. W. R. Grove, Phil. Trans. Roy. Soc. Lon. 142, 87, (1852).

2. N. D. Morgulis and V. D. Tischenko, Izv. Akad. Nauk SSSR, Ser. fiz., Vol. 20, No. 10, (1956).

3. S. P. Wolsky, Phys. Rev. 108, 1131 (1957).

4. R. B. Stuart and G. K. Wehner, 1960, "Vacuum Symposium Transactions," p. 290, Pergamon Press, (1961).

5. D. McKeown, Rev. Sci. Instr. 32, 133, (1961).

6. D. McKeown, "The Design Parameters and Operational Characteristics of an Electrostatically Accelerated Molecular Beam," Convair-Astronautics Report ERR-AN-006, October 1960.

7. A. Theodore Finkelstein, "A High Efficiency Ion Source," Rev. Sci. Instr. 11, 94, March 1940.

8. G. K. Wehner, "Advances in Electronic and Electron Physics," Academic Press, New York (1955).

9. S. Tolansky, Multiple Beam Interferometer, Oxford University Press, (1949).

10. D. McKeown, "Design Parameters for VHF Crystal Units," Proceedings of the Eleventh Annual Frequency Control Symposium, May 1957, Army Signal Research and Development Laboratories, Fort Monmouth, N. J. (1957).

11. W. P. Mason, Piezoelectric Crystals and Their Applications to Ultrasonics, p. 55, D. Van Nostrand Co., Inc., New York (1956).

12. H. D. Hagstrum, Rev. Sci. Instr., 24, 13 (1953).

13. G. Wehner, H. Laegrid, and R. V. Stuart, AFCRC Final Report No. 2133, "Study of Sputtering of Materials," Oct. 1960, General Mills, Inc., Minneapolis, Minn.

14. G. K. Wehner, ONR Report No. 1902, "Annual Report on Sputtering Yields," May 1959, General Mills, Inc., Minneapolis, Minn.

15. H. D. Hangstrum, Phys. Rev. 104, 3 (1956).

16. E. B. Henschke, Phys. Rev. 106, 737, (1957).

17. E. Langberg, Phys. Rev. 111, 91, (1958).

18. R. H. Silsbee, J. Appl. Phys. 28, 1246, (1957).

19. G. Leibfried, J. Appl. Phys. 30, 1388, (1959).

20. D. E. Harrison and G. D. Magnuson, Phys. Rev. 122, 1421, (1961).

DISTRIBUTION LIST

A. Government Distribution:

1. Department of Defense

Address	Copies
Office of the Director of Defense Defense Research and Engineering Information Office Library Branch Pentagon Building Washington 25, D. C.	2 copies
Armed Services Technical Information Agency Arlington Hall Station ATTN: TIPCR Arlington 12, Virginia	5 copies

2. Department of the Navy

Address	Copies
Chief, Bureau of Weapons Technical Library Navy Department Washington 25, D. C.	
Chief, Bureau of Ships Code 300, Technical Library Navy Department Washington 25, D. C.	
Chief of Naval Research Office of Naval Research ATTN: Physics Branch Washington 25, D. C.	3 copies
Director U. S. Naval Research Laboratory Technical Information Officer Code 2000, Code 2021 Washington 25, D. C.	6 copies
Commanding Officer Office of Naval Research Branch Office 495 Summer Street Boston 10, Massachusetts	
Commanding Officer Office of Naval Research Branch Office 346 Broadway New York 13, New York	

Contract Administrator
Southeastern Area
Office of Naval Research
George Washington University
2110 "G" Street, N. W.
Washington 7, D. C.

Commanding Officer
Office of Naval Research Branch Office
86 East Randolph Street
Chicago 1, Illinois

Commanding Officer
Office of Naval Research Branch Office (Dr. Ed Edelsack, 1 copy)
1000 Geary Street
San Francisco 9, California

Commanding Officer
Office of Naval Research Branch Office
1030 East Green Street
Pasadena 1, California

Commanding Office
Office of Naval Research Branch Office 2 copies
Navy #100 Box 39 Fleet Post Office
New York, New York

U. S. Navy Radiological Defense Center
San Francisco, California

Librarian
U. S. Naval Post Graduate School
Monterey, California

Commanding Officer
U. S. Naval War College
Newport, Rhode Island

Director
Research Department
U. S. Naval Ordinance Laboratory
White Oak, Silver Spring, Maryland

Commanding Officer
Physics Division
U. S. Naval Ordinance Test Station
Inyokern, China Lake, California

Commanding Officer
U. S. Naval Ordnance Laboratory
Corona, California

3. Department of the Air Force

Commanding Officer
Wright Air Development Division
Air Research and Development Command
U. S. Air Force
Wright-Patterson Air Force Base
Dayton, Ohio

AFSWC, SWRP
Kirtland Air Force Base
New Mexico

Headquarters
Air Force Cambridge Research Laboratories
Air Force Research Division (ARDC) (USAF)
Geophysics Research Directorate
Laurence G. Hanscom Field
Bedford, Massachusetts

4. Department of the Army

Commanding Officer
U. S. Army Engineering Research and
Development Laboratories
Fort Belvoir, Virginia
ATTN: Technical Intelligence Branch

U. S. Army Research Office
Box CM, Duke Station — 2 copies
Durham, North Carolina

U. S. Army Signal Engineering Laboratory
Fort Monmouth, New Jersey — 2 copies
ATTN: Technical Information Officer

Dr. J. L. Martin
Watertown Arsenal
Watertown 72, Massachusetts

5. Department of Commerce

Director
National Bureau of Standards
Washington 25, D. C.

Director
National Bureau of Standards
Boulder, Colorado

6. Other Agencies

Advanced Research Projects Agency
The Pentagon
Room 3E157
Washington 25, D. C.

National Aeronautics and Space Administration
1520 "H" Street, N. W.
Washington 25, D. C.

National Research Council
Division of Physical Sciences
National Academy of Sciences
Washington 25, D. C.

Director
National Science Foundation
Washington 25, D. C.

U. S. Atomic Energy Commission
Technical Information Service
P. O. Box 62
Oak Ridge, Tennessee

Defense Atomic Support Agency
Sandia Base, New Mexico

Defense Atomic Support Agency
Washington 25, D. C.

Professor R. B. King
California Institute of Technology
Department of Physics
Pasadena, California